Journal of Engineering and Sustainable Development
http://jeasd.uomustansiriyah.edu.iq/index.php
https://doi.org/10.31272/jeasd.26.2.7

Vol. 26, No. 02, March 2022
ISSN 2520-0917

VIRTUAL CFRP STRENGTHENING OF NON-PRISMATIC RC BEAMS WITHOUT LATERAL REINFORCEMENT

Ali Hameed Aziz

Civil Engineering Department, College of Engineering, Mustansiriyah University, Baghdad, Iraq

Received 3/9/2021 ***Accepted in revised form 6/11/2021*** ***Published 1/3/2022***

Abstract: The provision of the international codes does not cover clearly the design of non-prismatic reinforced concrete beams and the design has been left to the experience and judgment of design engineers. In the present paper, four beam specimens were cast and tested, one of which was poured as a prismatic beam (reference beam), while, the others were poured with non-prismatic sections. Virtual strengthening with bonded CFRP strips was adopted as an alternative technique instead of the real lateral reinforcement (stirrups) to evaluate the degree at which the load-carrying capacity of tested beam specimens was enhanced. Finite element method, as a numerical solution by ANSYS software, was adopted to simulate all the tested beam specimens which presented as three-dimensional problems. Experimental results show that the degradation due to tapering was varied between (50-94%) and (53-81%) for the ultimate and cracking load respectively, in comparison with the reference beam. While the analysis results indicated that the adopted technique plays important parameters to enhance the performance of the strengthened beams and the presence of CFRP increased the strength in the case of stirrups-less beams.

Keywords: *Shear, Non-Prismatic, RC Beams, ACI-318, Ansys, CFRP*.

1. Introduction

The applications of non-prismatic sections cover various fields in construction industry (buildings, long spans halls, bridges, towers, RC trusses, …..ect.). The esthetic shape (beauty of their shape) and saving in weight of non- prismatic reinforced concrete beams leads to use such member extensively in buildings and bridges construction. Due to the change in beam cross-section (throughout the beam length) and discontinuity of its slope, or the centroidal axis, non-prismatic members behave differently from prismatic ones. Several studies have looked at the effect of variation of the cross-section on the structural behavior, normal and shear stresses distribution, ultimate capacity in non-prismatic structural members. [1, 2, 3 and 4].

The reduction in shear capacity is effected significantly by beam action versus arch action mechanism (size effect, differences in behavior and mode of shear transfer at failure) [5] and [6].

**Corresponding Author*: alihaziz@uomustansiriyah.edu.iq

Work of This Research is Licensed under CC BY

Figure 1. Non-Prismatic RC beams under construction (North Tikrit Bridge)

Members of frames and continuous construction have to be constructed for the maximum impacts of factored loads as established by the theory of elasticity, according to building codes. Most structures are made up of prismatic members for cost considerations, and the size of each element is determined by the highest shear, torsion, axial stress, and bending moment along the span. Non-prismatic elements are occasionally addressed in structural systems, but designers normally model them using a restricted number of prismatic segments during analysis and subsequent design. Despite the widespread usage of non-prismatic reinforced concrete beams in buildings and bridges, there are no particular recommendations in current regulations, such as the International Building Code ACI-318M08 [7] or BS-5400-1 [8]. As a result, the design of the reinforced concrete non-prismatic beams depends mainly upon experience along with the judgment of design engineer. For the lateral stiffness, the structural engineers pay particular attention to the adequate modeling of non-prismatic RC beams. Generally, the shear capacity of non-prismatic members estimated by treated such members as prismatic elements considering the maximum effective depth at the deepest point. As a result, the structural analysis is cumbersome and the design criteria are nonexistent and the construction can expensive. During the working life (service age) of RC members they can deficient or distorted, due to several reasons, which means the requirements for the repairing or strengthening arise. The needed for repairing or strengthening may arise as a result of construction or design flaws, modifications of structural member function, updates in design standards and codes, maintenance lack, structural system change, increasing highway-volumes (for bridges), explosions, earthquakes, fires, accumulated damage and accidental overloading.

2. Research Significant

There are few researches about reinforced concrete non-prismatic beams and there shear failure mechanisms is not well understood, especially when the section without lateral reinforcement (stirrups).

3. Experimental Work

Four simply supported beam specimens, both prismatic and non-prismatic, were investigated and loaded under the effect of single monotonic load concentrated at the top face in mid-span. To insure failure in shear, the tested beams are reinforced longitudinally only without lateral reinforcement (stirrups). The varying in section is the major adopted variable. For all tested beams, the beam length, shear span-depth ratio (a/d), longitudinal reinforcement, and concrete class were all kept without any change. The experimental program also includes the casting and testing of a set of control specimens to determine the compressive strength of concrete (cubes).

3.1. Description of Tested Beams

Fig. 1 and Fig. 2, as well as Table (1), illustrate the nominal dimensions and details of the tested beams. The beams length and beams width were (1220mm) and (140mm) respectively. It may be noted that the depth of tested beams were kept constant at the right side end at (250mm) and varied from (150-250mm) at the left side end. At the bottom of all beam specimens, (2ϕ16 mm) bars were used as tension (flexural) reinforcement.

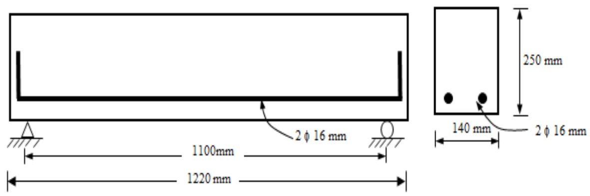

Figure 2. Prismatic beam (PB)

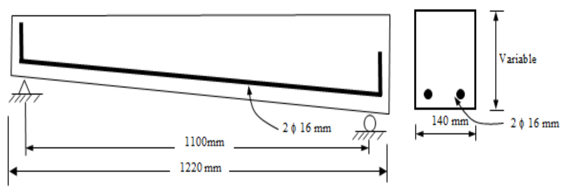

Figure 3. Non-prismatic beam (NPB)

The first beam specimen, (PB), is poured with constant depth (prismatic), while the beam specimens (NPB-1) is poured as a non-prismatic beams (varying depth of (250mm) at the right hand side and decreased gradually to (200mm) at the left hand side). While, the sample (NPB-2) and the sample (NPB-3) were cast with varying depth of (250mm) at right hand side and decreased gradually to (175mm) and (150mm) at left hand side respectively; details of the adopted dimensions and tapered angles are described in Table (1).

Table 1. Beams dimension with coding

Beam Code	(PB)*	NPB-1	NPB-2	NPB-3
L (mm)	1220	1220	1220	1220
b_w (mm)	140	140	140	140
h_L (mm)	250	200	175	150
h_R (mm)	250	250	250	250
h_L/h_R	1.0	0.8	0.7	0.6
Tapered Angle (α)	0°	2.35°	2.52°	4.69°

* Reference Beam

3.2. Properties of Materials

For manufacturing of the tested beam specimens, multi-use cement (OPC-Type I); sand from natural resources with smooth texture and rounded particle form with (2.12) as a fineness modulus; crushed, from natural resources, gravel with (10mm) of maximum size; clean potable water, from the water-supply network system, were used. The proportions of the used concrete mix per one cubic meter were (500kg), (750kg), (900kg), (100kg) and (150liter) for cement, sand, gravel, limestone and water respectively. It may be noted that, the used cement and aggregate (fine and coarse) were conformed to Iraqi specification (IQS 5/1984)[9] and (IQS 45/1984)[10], respectively.

Tensile strength test was performed for (ϕ16mm) deformed steel bars, which was used as a flexural reinforcement at the bottom. The tests were conformed according to ASTM A370-02 [11]. The results of tensile test indicated that the used steel bars has (f_y=491MPa), (f_u=653MPa) with (16%) elongation.

3.3. Concrete Mixing, Placing and Curing

One wooden mold of dimensions of (1220x140mm) for the length and width and variable depth was used to cast the samples. Concrete mixer with capacity of (0.2m^3) is used to mix the raw material of concrete. Once the mixing procedure was completed, the tested beams along with the control samples were poured then compacted directly. After (24hours), the samples were tearing from the molds and cured for (28days) at the laboratory temperature. Before (24hours), from testing date, the samples were removed from the curing container, and moved to the next stage; testing based on adopted methodology.

Figure 4. Beam specimen stripping and curing

3.4. Control Specimens Compressive Strength

BS 881-116 [12] with cubes of (150mm) is adopted to evaluate the concrete compressive grade (f_{cu}). Test results indicated that the compressive strength for cubes was (f_{cu}=24MPa). It may be noted that, the equivalent compressive strength of cylinder is required for finite element analysis, therefore, (f'_c=0.85 f_{cu}) is used to convert the compressive strength values.

3.5. Beam Specimens Testing

The beam and control specimens were both tested using a hydraulic testing machine. The mid-span deflection was measured using a dial gauge with (0.01mm) and (30mm) accuracy and capacity, respectively. The beam specimens were tested up to the failure, at ages of (28) days, under the action of monotonic load. The tested beams were, simply supported over (L_c=1100mm); Fig. 5 described beam specimens setup.

Loading was done gradually and in increments; the deflection, cracks development and cracks propagation (on beam faces) were observed and recorded during loading. Smaller increments were applied until the beams failed when they reached an advanced degree of loading. The tested samples were failing suddenly and the diagonal cracks expand wider, then, the loading machine stopped recording more, the deflection increase rapidly without any increasing in corresponding applied load. At each load increment, the development of cracks pattern was marked with a pencil.

Figure 5. Beam specimen setup

4. Finite Element Analysis

4.1. Element Selection and Modelling

To perform the virtual CFRP strengthening and to study more thoroughly the structural behaviour of the experimental, numerical analyses by ANSYS (version-12) finite element software [13], were investigate. To reach the required targets, the finite element analysis includes, in addition to verifications the tested beams, modelling of four CFRP hypothetically strengthened beam specimens, Table (2).

Table 2. Description of Finite Element Models

Beam Coding	Description	Strengthening by CFRP
PB-FE	F E Simulation of	None
PB-FES	Beam (PB)	Yes
NPB-1FE	F E Simulation of	None
NPB-1FES	Beam (NPB-1)	Yes
NPB-2FE	F E Simulation of	None
NPB-2FES	Beam (NPB-2)	Yes
NPB-3FE	F E Simulation of	None
NPB-3FES	Beam (NPB-3)	Yes

The concrete is modelled using brick, eight-nodes, nonlinear element (SOLID65) with 3DOF of translation type per element node. Axial, discrete, two-node element (LINK8) with 3DOF of translation type per element node is employed for FEM modelling of the steel reinforcement. The CFRP composite is modelled using 3DOF element node, (SHELL41), with in-plane (membrane) stiffness. For geometrical parameters modelling, steel bars cross-sectional area and shell element thickness should are input as real constants, as required in ANSYS software. To represent constitutive materials behaviour and features, material properties, which depends upon the mechanical properties such (f_y), (E), (υ) and (σ-ε) relationship, are required.

4.2. Material Modelling

For modeling of concrete, the SOLID65 element requires linear and multi-linear isotropic material properties. The multi-linear curves were used to help with convergence of the nonlinear solution algorithm. For concrete modeling, the compressive stress-strain curve was evaluated using the equations adopted by Desayi, P. and Krishnan, S. [14], Kachlakev, D. [15] and Wolanski, B.S. [16] to compute isotropic, multi-linear compressive stress-strain relationship. The steel bar element were modeled as isotropic, elastic-perfectly plastic, in tension and compression. CFRP composite material has directional characteristics. The unidirectional lamina has three mutually orthogonal planes of material qualities (xy, xz, and yz planes). The principal material coordinate axes were xyz. The x-direction is the fiber direction, and the y and z directions are perpendicular to the x-direction. The fiber direction may be considered as an isotropic material. The stress–strain relationships are roughly linear for CFRP strips up to failure. The manufacturer data of Sika Wrap Hex-230C was used for the finite element modeling of CFRP strips [17]. It is a strengthening or repairing system for structural members such as reinforced concrete, masonry, or wood. The company that provided this system was (Sika Near-East, Beirut-Lebanon). The data related to this system is summarized in Table (3).

Table 3. SikaWrap Hex-230C [17]

Property	Value (Description)
Fiber angle	0º (unidirectional).
Areal weight	225 g/m^2
Fabric thickness	0.13 mm
Fibers Tensile strength	3500 MPa
Fibers Tensile E-modulus	230 GPa
Break Elongation	1.5 %
Length/Roll of Fabric	≥ 45.7 m
Width of Fabric	305/610 mm

4.3. Beam Specimens Modelling and Meshing

The first step of modeling of the beam includes creation of blocks of the concrete volume; the concrete volume is created by pinpointing key-points of one side edge of the concrete block, then creating lines between these key-points to create the area, then forming by extruding these areas in the third dimension. After volumes identifying, meshing is required for numerical analysis. To obtain good consequences, the models were divided (meshing) into a number of small square or rectangular elements, Fig. 6.

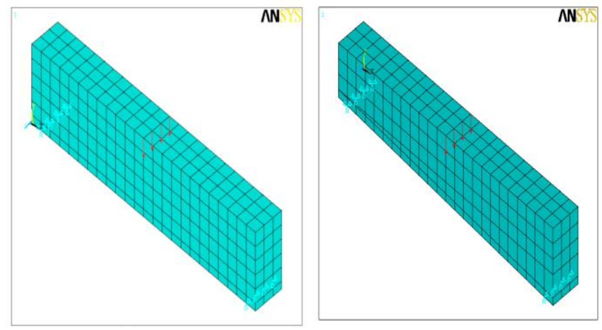

Figure 6. FE modeling of prismatic and non-prismatic beams

Throughout beams modeling, the steel bars were included and represented within the properties of eight-node concrete brick elements assuming full bond between both elements. To provide the full bond, the nodes of steel bar element (Link8) were connected directly within the adjacent nodes of solid elements (Solid65); this means the steel bar and concrete elements share the same connection nodes. To represent CFRP strips for strengthened beams, shell element has been used. No volumes meshing is needed such as for concrete, but individual four nodes elements are introduced (in the model) through the nodes of the surface which created by the volumetric concrete meshing. The CFRP strips were modeled as vertical strips with spacing of (150mm). Full bond between CFRP elements and concrete elements is assumed (because the CFRP elements are created throw the nodes of concrete elements); therefore, no contact elements is needed for epoxy material modeling.

4.4. Boundary Conditions and Loads

To obtain a unique numerical solution, the boundary conditions of displacement are necessary to constrain the FE models. To certify that the model acts the same way as the experimental specimens, boundary conditions need to be applied at the points of supports. The boundary condition includes restrained the movement in x, y, and z for left support to obtained the hinged support. From the other hand, for the right support, the roller support is obtained by constraining nodes in y-z-direction at the bottom face; Fig. 7.

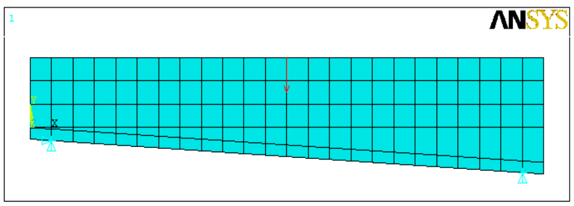

Figure 7. Creation of model boundary condition

It may be noted that, due to absent of the rotational degrees of freedom, in both boundaries, the rotation was allowed. The load was applied along entire centerline (at the top); thus, the applied load should be divided into equivalent nodal forces at the position of the top nodes. Therefore, the equivalent force at each node on the plate was (1/4) of the actual force applied per nodes number.

The load is separated into load steps and applied in stages until the failure (based on Newton-Raphson technique). At a certain stages in the analysis, load step size is varied from large (at points of linearity in the response) to small (when cracking and steel yielding occurred).

When the load reaches the final step of loading and the phrase (solution is done!) appears on the software screen, the analysis is assumed to be completed. Otherwise, when the solution for a minimum load is diverging and the models have a high deflection, the failure is assumed to have occurred.

4.5. Properties of Construction Material

Mechanical tests such as modulus of elasticity, yield stress, Poisson's ratio, and stress-strain relationship are used to characterize the behavior and features of constitutive materials. However, each of the given types of elements has a set of basic parameters that may be found in the ANSYS elements library. The values of those element parameters are required for a similar depiction of each tested beam, as they are utilized to approximate real constants and material properties. In the present paper, the adopted elements property parameters are reported in Appendix -A-.

5. Results and Discussion

5.1. Behaviour and Strength of Beams

As mentioned before, the experimental work consist casting and testing of four reference beams that are free of any strengthening strips, one parameter was adopted which was tapered angle (α). The test results are provided and listed in Table 4, while the cracks patterns and failure modes of reference beams (experimentally tested beams) are shown in Fig. 8.

Table 4. Experimental results

Beam Coding	P_{cr} (kN)	P_u (kN)	P_{cr}/P_{crR} (%)	P_u/P_{uR} (%)	Δ_u (mm)
PB	32	80	1.00	1.00	2.7
NPB-1	26	75	0.81	0.94	2.6
NPB-2	21	62.5	0.66	0.78	2.4
NPB-3	17	40	0.53	0.50	2.35

(a) (b)

(c) (d)

Figure 8. Crack pattern of tested beam specimens
(a) PB (b) NPB-1; (c) NPB-2; (d) NPB-3

Tapered angle effect appeared mainly on the load capacity of the tested tapered beams, increasing (α) leads to decrease in the first inclined shear cracking (P_{cr}) and ultimate shear load (P_u) values as they considered a function of tapered angle "when the tapered angle increases, the volume of concrete diminishes, therefore, the shear strength also diminishes" [8]. Degradation due to tapering were varied between (50-94%) and (53-81%) for the ultimate and cracking load capacity respectively, in comparison with the reference beam specimen (PB). Fig. 9 shows the degradation curve of the ultimate strength due to variation of tapering (h_L/h_R ratio).

The experimental evidences show that the diagonal cracks extended from supports towards the load position, the failure take place due to diagonal tension cracks were formed diagonally, in the side of the shallow shear span, and moved up and towards the position of load, this crack is associated with crushing of the concrete near the positions of the applied loads, this mode of failure is called "Shear-Compression" failure, as shown in Fig. 8.

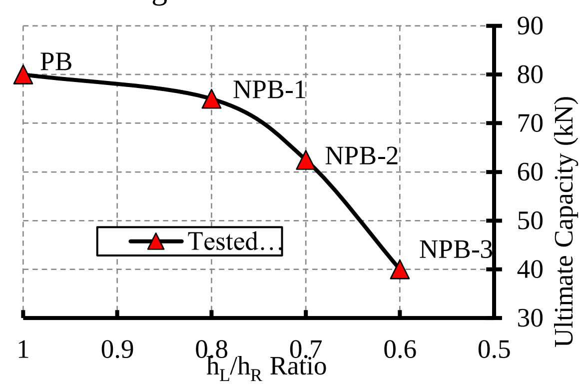

Figure 9. Degradation of ultimate strength due to tapering

5.2. Effect of Tapered Angle (α) on Load-Deflection

Load-deflection curves of the tested beams at mid-span at all stages of loading up to failure are constructed and shown in Fig. 10. All curves are identical at first, and the tested beams show linear behavior. The initial change in slope of the load-deflection curves occurs between (10 kN and 30 kN), indicating the first cracking load. Beyond the first cracking load, each beam behaved in a certain manner due to the effect of the tapered angle which appeared clearly on the load-deflection curves of the tested beams, where deflection undergoes a noticeable increment as the value of (α) increase. In comparison to the other beams, the behavior of the reference beam (PB) showed higher loads and deflections. The reference beam (PB) has a greatest stiffness due to uniform section. Load-deflection curves for the tested beams (NPB-1, NPB-2 and NPB-3) exhibits smooth increase in both applied loads and deflections. Gradual reduction in depth caused decreasing in the load carrying capacity beyond the first cracking, this associated with reduction in beams stiffness and this is reflected on the corresponding deflections (excessive deflection).

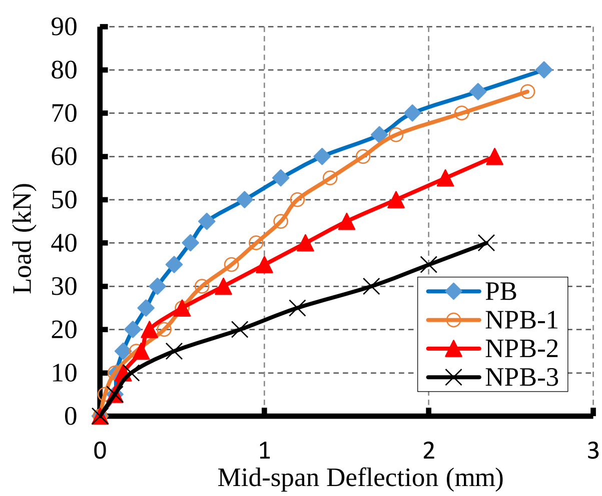

Figure 10. Effect of (α) on deflection of experimentally tested beams

5.3. Effect of Strengthening Scheme on Beams Behavior

5.3.1. Ultimate Load Capacity

The numerical results obtained, for non-strengthened FE models; using ANSYS finite element is relatively identical to the experimental ones, showing reasonable agreement with variation of range (5%-15%) in all the specimens. From the other hand, for strengthened FE models, the analysis evident show that the presence of CFRP strips significantly enhanced the ultimate load for all cases; The ultimate capacity were enhanced by 28%, 43%, 50%, and 55% for the FE models PB-FES, NPB-1FES, NPB-2FES and NPB-3FES respectively. The observed enhancement in ultimate load is due to contribution of both, CFRP strips in tension range and the concrete in the compression range to resist diagonal tension stresses, which governed the mode of failure. Table 5 provided the numerical analysis results and comparison of each beam model.

Table 5. Finite Element Analysis Results

Beam Coding	Pu (kN)	$(P_u)_{FE}/(P_u)_{EXP}$	Mode of Failure
PB-FE	85	1.06	Shear- Failure
PB-FES	102	1.28	Shear- Failure
NPB-1FE	79	1.05	Shear- Failure
NPB-1FES	100	1.43	Shear- Failure
NPB-2FE	70	1.12	Shear- Failure
NPB-2FES	94	1.50	Shear- Failure
NPB-3FE	46	1.15	Shear- Failure
NPB-3FES	62	1.55	Shear- Failure

5.3.2. Load-Vertical Displacement (Deflection)

Load-vertical displacement (deflection) curves of experimentally tested beams and FE models are provided in Fig. 11. The presence of CFRP in the tapered beams at the shear span leads to reduction in deflection, at same load level, when compared with the corresponding beams without strengthening. Also, all strengthened models show more energy absorption due to extended of load-deflection curves which led to increase the area under the curves.

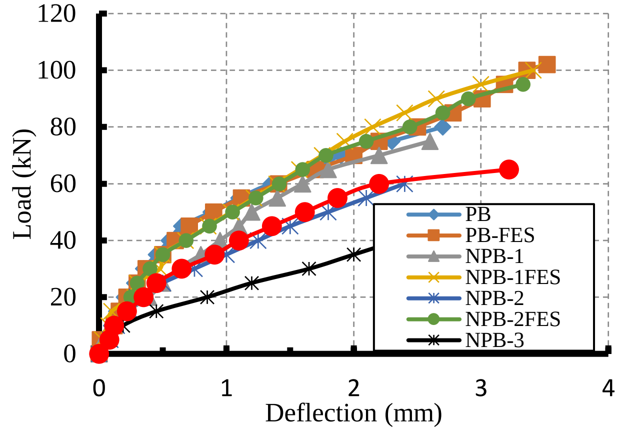

Figure 11. Load-deflection of experimentally tested beams and FE models

5.3.2. Crack Pattern of FE Models

The crack pattern is recorded by the ANSYS program at each applied load step. The finite element analysis and the experimental response for the beam crack patterns are very similar, as illustrated in Fig. 12. The FE models properly predict that tested beams will failed in shear, with vertical and inclined cracks appearing in the shear span zones. The cracks are clustered at the shear span and disappear diagonally toward the beam supports.

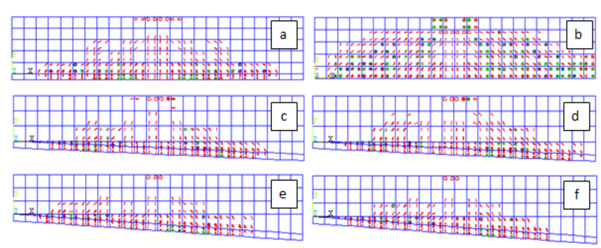

Figure 12. Crack patterns from FE models (a) PB-FE;

(b) PB-FES; (c) PB-1FE; (d) PB-1FES; (e) PB-3FE; (f) PB-3FES

6. Conclusions

1- For non-prismatic tested beams, the first inclined cracking and ultimate shear strength depends mainly on tapered angle;

the experimental results show that, the increasing tapered angle leads to a reduction in ultimate load capacity by (50%) and produced higher deflection values.

2- The crack patterns at the final loads from the finite element models compared well with the observed failure modes of the experimental beams, and the general behavior of the finite element models represented by the load-deflection curves at mid-span shows good agreement with the test data of the experimentally tested beams..

3- For non-strengthened FE models the numerical results showing reasonable agreement in ultimate load capacity with variation of range (5%-15%). While, for strengthened FE models, a significant improvement in ultimate load capacity, for all cases, with variation of range (28%-55%) were recorded. The load capacity of each simulated RC beams were properly predicted using finite element models.

4- The presence of CFRP in the tapered beams at the shear span produce a significant reduction in deflection, at the same load level, when compared with the corresponding beams without strengthening.

Conflict of interest

The author confirms that the publication of this article causes no conflict of interest.

7. References

1. Debaiky, S. Y., Niema, E. I. (1982) "*Behavior and Strength of Reinforced Concrete Haunched Beams in Shear*", ACI Structural Journal, Vol. (79), Issue (3), 184-194.
2. El-Niema, E. I. (1988) "*Investigation of Concrete Haunched T-beams under Shear*", ASCE Journal of Structural Engineering, Vol (114), Issue (4), 917-930.
3. MacLeod, I. A., Houmsi, A. (1994) "*Shear Strength of Haunched Beams without Shear Reinforcement*", ACI Structural Journal, Vol. (91), Issue (4), 79-89.
4. Tena-Colunga, A., Archundia-Aranda, H.I., González-Cuevas, Ó.M. (2008) "*Behavior of Reinforced Concrete Haunched Beams Subjected to Static Shear Loading*", Engineering Structures, Vol. (30), Issue (2), 478-492.
5. Sneed, L. H., Ramirez, J. A. (2010) "*Influence of Effective Depth on Shear Strength of Concrete Beams-Experimental Study*", ACI Structural Journal, Vol. (107), No. (5), 554–562.
6. Bazant, Z. P., Kazemi, M. T. (1991) "*Size Effect on Diagonal Shear Failure of Beams without Stirrups*", ACI Structural Journal, Vol. (88), No. (3), 268–276.
7. ACI Committee 318, (2008) "*Building Code Requirements for Structural Concrete*", (ACI 318-M08) and Commentary (ACI 318R-08), American Concrete Institute, Farmington Hills, MI, pp.465.
8. BS 5400-1, (1988) "*Steel, Concrete and Composite Bridges-General Statement*", British Standards Institute, London, UK.
9. Iraqi Specifications No. (5), (1984) "*Portland Cement*", Iraqi Central Organization for Standardization and Quality Control, Baghdad-Iraq.
10. Iraqi Specifications No. (45), (1984) "*Aggregates from Natural Sources for Concrete and Building Construction*", Iraqi Central Organization for Standardization and Quality Control, Baghdad-Iraq.
11. ASTM A370-02. (2002). "*Standard Test Methods and Definitions for Mechanical Testing of Steel Products*", ASTM

International, West Conshohocken, PA, USA.

12. BS 1881-116, (1983) "*Method for Determination of Compressive Strength of Concrete Cubes*", British Standards Institute, London, UK.
13. ANSYS Manual, Version (12).
14. Desayi, P., Krishnan, S. (1964) "*Equation for the Stress-Strain Curve of Concrete*", ACI Journal, Proc. 61(3), 345-350.
15. Kachlakev, D. (2002) "*Finite Element Analysis and Model Validation of Shear Deficient Reinforced Concrete Beams Strengthened with GFRP Laminates*", California Polytechnic State.
16. Wolanski, B.S. (2001) "*Flexural Behavior of Reinforced and Pre-Stressed Beams Using Finite Element Analysis*", M.Sc. Thesis, Marquette University, (73) p.
17. Jasem, M. A. (2018) "*Shear Behavior of Reinforced Self-Compacting Concrete Hollow T-Beams with Different Hollowness Ratio*", M.Sc. Thesis, College of Engineering, Mustansiriyah University, Baghdad, Iraq.

Appendix-A- Elements Property Parameters

Element	Parameter	Description		Value
Solid 65	f_c'	Compressive strength (MPa)		-1
	f_t	Tensile strength (MPa)		4.32
	*βo	Open coefficient of shear transfer		0.3
	*βc	Close coefficient of shear transfer		0.6
	Ec	Young's modulus of elasticity, MPa		29142
	υ	Poissons ratio		0.2
Link 8	A_b	Cross section Area (mm^2)		79.5
	f_y	Yield stress (MPa)		418
	E_s and E_t	Elasticity modulus (MPa)	E_s	200000
		Modulus of strain hardening (MPa)	E_t	0
	υ	Poisson's ratio		0.3
Shell 41	t	Thickness(mm)		0.13
	f_y	Yield stress (MPa)		3500
	E_f	Modulus of Elasticity-E_f (GPa)		230